The size of the PROM can be substantially reduced by comparing the two variables to determine the larger ($L$) and smaller ($S$):

$$\log_2 (I^2 + Q^2) = \log_2 L + \log_2 (1 + S^2/L^2) \tag{3.16}$$

The latter term of Eq. (3.16) requires fewer bits than that of Eq. (3.15) because its maximum value is 3 dB. The PROM address also is unipolar and may be limited at a ratio where the PROM output drops to zero.

The log power combiner makes power (square-law) integration feasible. A number of variables may be weighted by addition of logarithmic scaling factors and successively accumulated, using the log power combiner to combine each with the prior partial power summation. Square-law integration of multiple echoes from a target provides better sensitivity than prior methods, but this was impossible with analog signal processing and costly when using conventional digital processing.

## 3.9 IF LIMITERS

**Applications.** When signals are received that saturate some stage of the radar receiver which is not expressly designed to cope with such a situation, the distortions of operating conditions can persist for some time after the signal disappears. Video stages are most vulnerable and take longer to recover than IF stages; so it is customary to include a limiter in the last IF stage, designed to quickly regain normal operating conditions immediately following the disappearance of a limiting signal. The limiter may be set either to prevent saturation of any subsequent stage or to allow saturation of the A/D converter, a device which is usually designed to cope with modest overload conditions.

The IF phase detector described in Sec. 3.10 requires a limiter to create an output dependent on phase and independent of amplitude. It is employed in phase-lock servos and phase-monopulse receivers.

An IF limiter is sometimes employed prior to doppler filtering to control the false-alarm rate when the clutter echo is stronger than the filter can suppress below noise level. This was widely used in early two-pulse MTI, but it has drastic impact on the performance of the more complex doppler filters of modern radars. It is only compatible with phase-discrimination constant false-alarm rate (CFAR; Sec. 3.13), but it serves a useful purpose in radars utilizing this CFAR process after doppler filtering.

**Characteristics.** The limiter is a circuit or combination of like circuits whose output is constant over a wide range of input signal amplitudes. The output waveform from a bandpass limiter is sinusoidal, whereas the output waveform from a broadband limiter approaches a square wave.

There are three basic characteristics of limiters whose relative importance depends upon the application. They are performance in the presence of noise, amplitude uniformity, and phase uniformity. When the input signal varies over a sufficiently wide range, all these characteristics become significant. Amplitude uniformity and phase uniformity are dependent largely on the design of the limiter and are a direct measure of its quality.

*Noise.* Limiter performance in the presence of noise is characterized by a failure to limit signals buried in noise and by an output signal-to-noise ratio that

differs from the input signal-to-noise ratio. Gardner[10] gives an approximate but useful relation for bandpass limiters which demonstrates the effect of limiting on the signal-to-noise power ratio when both are present simultaneously.

$$\left(\frac{S}{N}\right)_0 = \left(\frac{S}{N}\right)_i \frac{1 + 2(S/N)_i}{4/\pi + (S/N)_i} \tag{3.17}$$

$$\left(\frac{S}{N}\right)_0 = 2\left(\frac{S}{N}\right)_i \qquad \text{when } \left(\frac{S}{N}\right)_i \gg 1 \tag{3.18}$$

This is the result of limiter suppression of the in-phase noise component, leaving only the quadrature component to compete with the signal.

$$\left(\frac{S}{N}\right)_0 = \frac{\pi}{4}\left(\frac{S}{N}\right)_i \qquad \text{when } \left(\frac{S}{N}\right)_i \ll 1 \tag{3.19}$$

This slight suppression of weak signals by the noise approximates the degradation of detectability that can be attributed to the limiter in the phase-discrimination CFAR techniques described in Sec. 3.13. Strictly speaking, these equations do not apply to the detection of pulsed radar echoes; they do not relate to the probability distributions of signal plus noise compared with noise alone. However, as the bandwidth-time product at the limiter increases, Eq. (3.19) defines the effect on the minimum detectable signal more and more closely.

Gardner also demonstrates the relation between output power and $(S/N)_i$:

$$S_0 \approx \frac{(S/N)_i}{4/\pi + (S/N)_i} \tag{3.20}$$

When $(S/N)_i \gg 1$, the output signal power is seen to be constant; however, when $(S/N)_i \ll 1$, the output signal power is seen to be a linear function of input signal power. This is of considerable importance in the design of phase-lock loops.

*Amplitude Uniformity.* No single-stage limiter will exhibit a constant output over a wide range of input signal amplitude. One cause is apparent if one considers a single-stage limiter having a perfectly symmetrical clipping at $\pm E$. The rms output at the threshold of limiting is $E/2$, rising to the value $(4/\pi)(E/2)$ when the limiter is fully saturated and the output waveform is rectangular.

In a practical case, the amplitude performance is also affected by capacitive coupling between input and output of each limiting stage, charge storage in transistors and diodes, and *RC* time constants which permit changes in bias with signal level. For these reasons, two or more limiter stages are cascaded when good amplitude uniformity is required.

*Phase Uniformity (Phamp).* The change of phase with signal amplitude (phamp) of a limiter is more readily measured than analyzed. Calaway[11] bases some very useful conclusions on a series of experiments with five common limiter circuits. He demonstrates that a transistor provides maximum phase uniformity when used in the current-mode switching configuration and that the diode provides better overall performance in the series mode when charge storage effects are not evident.

In conventional limiter types known for their phase uniformity, there are two common denominators worth noting. In each case the peak-to-peak output can be

expressed as the product of a switched fixed current and a resistance; these limiters have been described as *available-power* switching types. Second, the phamp of any particular limiter circuit is generally directly proportional to the frequency at which it is operated; its variation with signal amplitude is better characterized by nanoseconds per decibel than by degrees per decibel.

## 3.10 PHASE DETECTORS AND SYNCHRONOUS DETECTORS

**Definitions and Characteristics.** The distinction between a phase detector, a synchronous or phase-sensitive detector, and a balanced mixer is sometimes unclear. This results from the similarity of analog circuits that perform these functions. It is generally agreed, however, that a particular circuit is used as a phase detector when only phase information is present in the output, as a synchronous detector where both phase and amplitude information is present in the output, and as a mixer when phase, amplitude, and frequency information is present in the output. Doppler frequency shifts are excepted in this convention.

Phase-detector output characteristics generally fall into one of the three classes shown in Fig. 3.16. Peculiarly, the characteristic of a given detector is not invariant. Gardner[10] shows three cases where the characteristic of a particular detector depends upon the shape of the applied signals. Certain types of diode detectors exhibit a sinusoidal characteristic with sinusoidal inputs and a triangular characteristic with square-wave inputs. In some cases a shift from the triangular to the sinusoidal characteristic accompanies a reduction in signal level or the introduction of noise.

In certain high-performance systems where maximum information is to be retained, a pair of synchronous detectors may be operated in quadrature. Their operation is described by the following diagram:

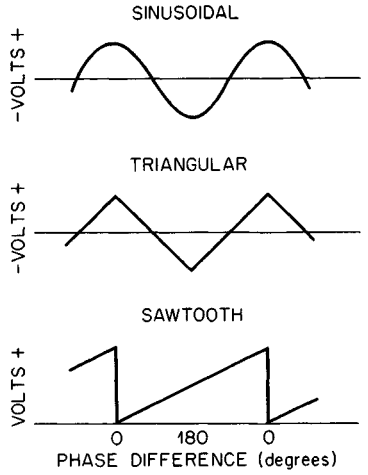


**FIG. 3.16** Phase-detector characteristics.

$$E_S \sin(\omega t + \theta) \longrightarrow \otimes \longrightarrow \frac{E_S E_R}{2} \cos\theta \qquad (3.21)$$

$$E_R \sin \omega t \uparrow$$

$$E_S \sin(\omega t + \theta) \longrightarrow \otimes \longrightarrow \frac{E_S E_R}{2} \sin\theta \qquad (3.22)$$

$$E_R \cos \omega t \uparrow$$

The in-phase ($I$) and quadrature ($Q$) operation is described by the first and second lines, respectively. If the detector produces a triangular rather than sinusoidal function of phase angle, the two outputs may still be described as in-phase and quadratic components, but they will be distinguished by quotation marks (*"I"* and *"Q"*). In this case, the detector operates as a phase detector rather than as a synchronous detector.

**Applications**

*MTI Radar.* A phase-sensitive detector is a key element in nearly all MTI radar systems. It is used to detect the echo vector phase shift produced by target motion between pulses. The reference signal to the detector is supplied by a second local oscillator, known as a coho because of its coherence with the transmitted signal. The phase detector allows the echo signal to be stored in the form of a video signal or arithmetic number representing the echo vector.

To reduce cost and maintenance, early MTI cancelers often possessed only one phase component. In such a canceler the triangular *"I"* component is used for large echoes, as this minimizes blind phase effects that occur in the $I$ characteristic, at the point where $dE/d\theta$ is near zero. For echoes below the limit level, the *"I"* characteristic converts to an $I$ characteristic, and blind phase effects are accepted. The *"I"* characteristic is unsuitable for cancelers using three or more pulses. This results from the dependency of the weighting on a smoothly varying doppler vector. In any case, the best performance results when both $I$ and $Q$ are used.

*Phase and Phase-Rate Trackers.* The phase detector is used to measure accurately the velocity of targets that have been isolated by other means. High accuracy results from the long time base used in the measurement. The $(N + 1)$st measurement of radial velocity is given by

$$V_{N+1} = \frac{c}{2\omega}\left(\frac{\phi_{N+1} - \phi_N}{\text{PRT}}\right) \qquad (3.23)$$

where $c$ = velocity of light
$\omega$ = radar angular frequency
$\phi_N$ = $N$th phase measurement
PRT = interpulse time

Extraction of this information in a practical case requires a filter, such as the tracking loop.

Figure 3.17*a* shows a phase tracker in which the predicted phase $\phi_P$ is continuously compared with the measured phase $\phi_M$. The velocity is extracted from the derivative of the predicted phase $\phi_P$. Because the tracker is measuring phase,

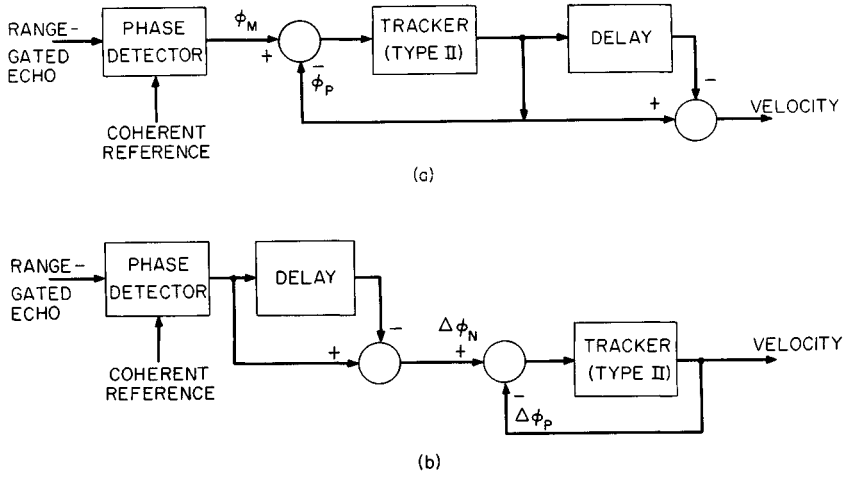


**FIG. 3.17** (*a*) Phase tracker. (*b*) Phase-rate tracker.

which is equivalent to range, the system is acceleration-limited and therefore does not have wide application.

Figure 3.17*b* shows a phase-rate tracker in which the predicted phase difference $\Delta\phi_P$ is continuously compared with the measured phase difference $\Delta\phi_M$. This is accomplished by taking the derivative of the phase ahead of the tracker. In this case the velocity is directly proportional to the predicted phase difference $\Delta\phi_P$. Because the tracker is measuring phase rate, which is equivalent to velocity, the system is not acceleration-limited. Lag errors are introduced only by the next higher derivative, jerk.

*Monopulse Angle Measurement.* In the monopulse radar, a pair of antenna horns are used to form two like beams, which point in slightly different directions. The two antenna ports are connected to a hybrid with sum and difference outputs. The antenna pattern of the difference port will exhibit a null directly between the beams, whereas the pattern of the sum port will exhibit a peak. These hybrid outputs are referred to as the difference signal ($\Delta$) and the sum signal ($\Sigma$).

Figure 3.18*a* illustrates the most common amplitude-comparison monopulse configuration. Automatic gain control derived from the amplified signal in the $\Sigma$ channel causes matched variable-gain amplifiers in both channels to have a gain proportional to $\Sigma^{-1}$. The amplified difference-channel signal $\Delta/\Sigma$ is synchronously detected to preserve phase polarity. This monopulse receiver is restricted to radars and targets that create only small variation in echo amplitude from one pulse to the next.

Figure 3.18*b* illustrates a monopulse receiver without this limitation. In this receiver, the amplitude information is converted into phase information by a quadrature hybrid. The hybrid outputs $A \pm jB$ and $A \mp jB$ are translated to IF frequency and ultimately phase-detected against each other. The phase detector for this application should have a sawtooth characteristic, in which case its output is

$$2 \sin^{-1} \frac{\pm B}{K}$$

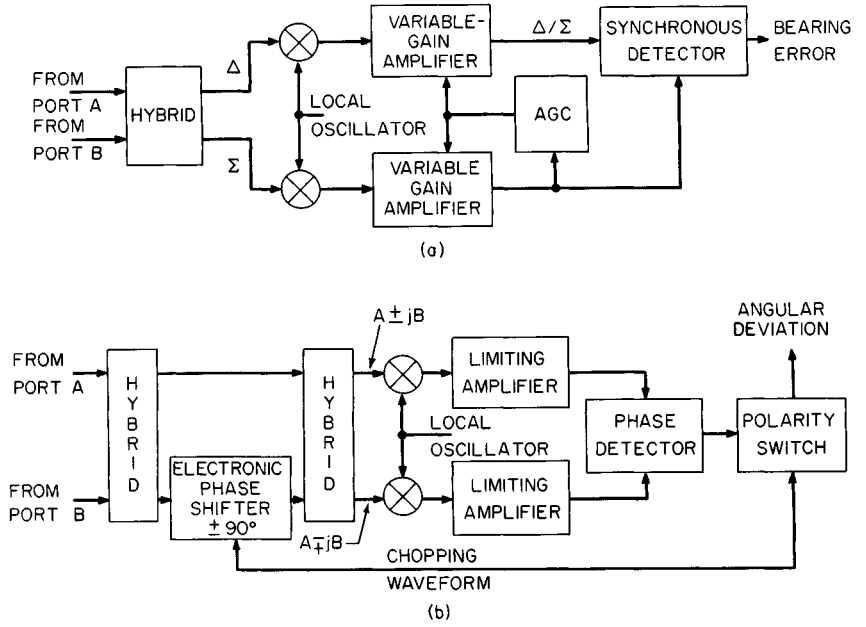


**FIG. 3.18** (*a*) Amplitude-comparison monopulse receiver. (*b*) Phase-comparison monopulse receiver.

where $K$ is a constant equal to $\sqrt{A^2 + B^2}$. The alternating polarity of $B$ is introduced by a phase chopper to allow for correction of receiver phase errors. It is removed by a reversing switch following the detector.

*Recording.* Radar echoes are sometimes recorded for subsequent analysis, usually by a digital computer. Digital recording prevents degradation of data in recording and also provides direct access to the computer. If the dynamic range is reasonably low, $I$ and $Q$ signals may be recorded. Where the dynamic range is large, phase and log amplitude may be used to minimize the number of bits. As an example, consider a system requiring 3 percent recording increments over a 72 dB dynamic range. $I$ and $Q$ recording requires two channels of 17 bits each, whereas phase- and log-amplitude recording for the same performance requires only 8 bits in both channels. Details of the comparison are given in Table 3.3.

**TABLE 3.3** Comparison of $I$ and $Q$ with Phase- and Log-Amplitude Recording

| Parameter | $I$ and $Q$ recording | Recordings of phase and log amplitude | |
|---|---|---|---|
| Least significant bit (LSB) | 1/32 | 0.03 rad | 0.28 dB |
| Most significant bit (MSB) | 4000 | 2 rad | 72 dB |
| MSB/LSB | 128,000 | 256 | 256 |
| Number of bits | 17 each | 8 | 8 |

### Examples of Phase Detectors

*Multiplier Detector.* The gated-beam tube and, to some extent, the beam-deflection tube have been used as analog multipliers to obtain the product of the signal and reference waveforms. They are self-limiting and produce a gradual transition from the *I* to "*I*" characteristics about the saturation level. When they are used as synchronous detectors, the dynamic range is restricted by the high noise level of these devices. This type of multiplier detector also may be implemented by using a field-effect transistor (FET) multiplier as suggested by Highleyman and Jacob.[12]

*Balanced-Diode Detector.* The balanced-diode detector of Fig. 3.19*a* is widely used because of its unusually favorable characteristics. When two sinusoids of frequency $\omega$ and phase difference $\theta$ are applied to this detector, the output is given by

$$E_{out} = K(\cos\theta - \cos 2\omega t + \text{higher-order terms}) \tag{3.24}$$

Under these conditions, the characteristic is sinusoidal, and the ripple is free from a fundamental component. When bandwidth permits, the detector will operate with square-wave inputs to give a triangular characteristic.

This circuit can be purchased in modular form, containing a pair of balanced wideband transformers and matched hot-carrier diodes. The detector can be obtained with 35 dB isolation between ports over a frequency range of 3 to 100 MHz. Units having a maximum frequency limit of 1 GHz are available.

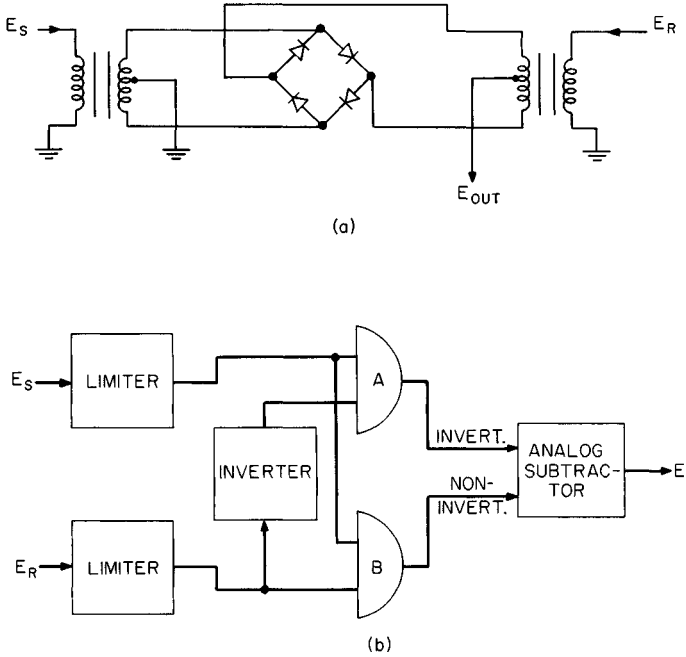


**FIG. 3.19** (*a*) Balanced-diode detector. (*b*) Coincidence phase detector.

In theory, the dynamic range is determined by the maximum signal-to-noise ratio at the output. In practice, however, it tends to be limited by unbalanced residuals and their fluctuation. Very precise detectors of this type may have a usable dynamic range of 50 dB.

*Coincidence Phase Detector.* The coincidence detector of Fig. 3.19*b* provides a triangular output characteristic. When $E_S$ and $E_R$ are in phase, AND gate *B* registers coincidence half the time, and AND gate *A* registers no coincidence. This condition leads to maximum negative output. When $E_S$ and $E_R$ are out of phase, the reverse condition exists, and maximum positive output results. Normally the triangular characteristic exhibits some rounding of the peaks. However, the detector has been built with very sharp peaks, using a tunnel-diode threshold in each channel.

The coincidence phase detector has a fundamental ripple-frequency component. A higher ripple frequency results from exclusive OR-gate logic, but this introduces voltage offsets that may be troublesome.

**Analog-to-Digital Phase Detector.** The phase detector of Fig. 3.20 measures the time interval between positive (or negative) zero crossings of the signal and reference waveforms. A pair of zero-crossing detectors generate sharp spikes at their respective points of crossing. The reference-channel spike sets a RESET-SET (*R-S*) flip-flop, and the signal-channel spike resets it. A gated oscillator generates a clock waveform while the flip-flop is in the SET state, and a counter measures the length of this interval. Filtering is accomplished by a buffer register.

The resolution of this phase detector is determined by the ratio of the clock frequency to the intermediate frequency $\omega_2$ of the signal. In a tracking radar with a range gate, the signal bandwidth may be narrowed drastically after gating with-

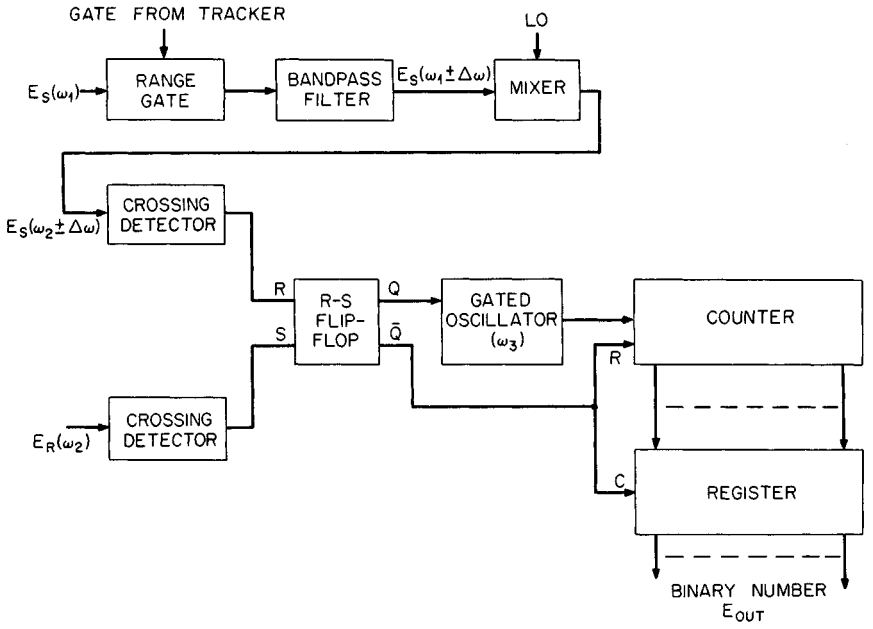


**FIG. 3.20** Analog-to-digital phase detector.

out loss in signal-to-noise ratio. The resultant signal may then be translated to a very low IF frequency without spectral foldover problems.

In this system, the filter receives a signal of short duration compared with its response time. It then rings at its own natural frequency, whose deviation ($\Delta\omega$) from the nominal frequency ($\omega_1$) must be very small if the sawtooth phase detector is to produce correspondence between the 0 and 360° points to within the least significant bit. Given the filter tolerance and the counter speed, the best accuracy is achieved by making the frequency at the crossing detector equal to their geometric mean.

This type of phase detector can be made fairly precise. However, it was noted by Gardner[10] in connection with a similar device that the signal quality must be high to ensure reliable operation of the flip-flop. The narrowband filter, which in effect samples and holds the phase, overcomes this problem.

**Digital Phase Detector.** In most modern radars, digital doppler filters are utilized to attenuate clutter interference prior to extracting the phase (and amplitude) of the desired target echo. The data is in digital form, with real ($I$) and imaginary ($Q$) components; so the phase detectors which have been discussed previously (requiring IF inputs) are inappropriate.

The phase is extracted most simply by converting the data to logarithmic format, by the methods described in Sec. 3.8. The phase-detector inputs then consist of polarities of $I$ and $Q$, $\log_2 I^2$, and $\log_2 Q^2$. The two polarities define the quadrant, and the phase within the quadrant is a PROM function of $\log_2 I^2 - \log_2 Q^2$.

Phase-discrimination CFAR (Sec. 3.13) tolerates crude phase information, and insignificant benefit results from extracting phase to better than 3 bits. A 3-bit digital phase detector may utilize either linear or log data to extract the octant merely by comparing the magnitudes of $I$ and $Q$. The PROM address consists of nine states:

$$I < 0 \qquad I = 0 \qquad I > 0$$

$$Q < 0 \qquad Q = 0 \qquad Q > 0$$

$$|I| < |Q| \qquad |I| = |Q| \qquad |I| > |Q|$$

It is important in this application[13] to maintain an equal probability of each phase output in noise; so the data corresponding to the boundary conditions [$I = 0$, $Q = 0$, or $|I| = |Q|$] must be assigned to the neighboring octant in a consistent rotational sense (either clockwise or counterclockwise). A pseudorandom phase output is necessary at the origin [$I = 0$, $Q = 0$].

The coded-pulse anticlutter system (CPACS) decoder[13] requires data in the form of $k \cos \phi$ and $k \sin \phi$ rather than phase ($\phi$). The conversion can be made by a second PROM. A 3-bit output is provided when $k = 7$; output states are 0, ±5, and ±7. A 2-bit output is provided when $k = 3$; output states are 0, ±2, and ±3, which introduces tolerable error.

## 3.11 ANALOG-TO-DIGITAL CONVERTER

**Applications.** Analog-to-digital converters find numerous applications in modern radar systems. The trend toward digital processing of radar data has resulted in a demand for fast converters that are able to convert data in real time.

Digital MTI is an example of a technique requiring such high-speed converters. Here, the synchronous-detector output is sampled at a rate not less than the receiver

bandwidth, and the digital result is stored in a large digital memory. Data is read from the memory to allow comparison with corresponding returns from subsequent radar "looks." The flexibility of this method has permitted MTI velocity response characteristics previously unobtainable with analog memory devices.

Many tracking radars use a converter to encode the echo in the tracking gate. In this case, a general-purpose computer provides all computations required to track a target and to provide range and velocity outputs. Precise data-smoothing and stabilizing characteristics are provided by the computer.

High-speed converters have been used to encode the height information from a stacked-beam radar. This permits an arithmetic interpolation of target position. Errors following conversion are, of course, eliminated.

Another application of converters is in the field of digital recording. This is used where vast quantities of data are to be analyzed or where an isolated event is to be analyzed. In this case, the encoded data is stored on magnetic tape. The results are then analyzed in nonreal time with arithmetic accuracy.

**Formats.** The most frequently used digital format is the power-of-2 binary forms:

$$E = K(b_N 2^{N-1} + b_{N-1}2^{N-2} + b_{N-2}2^{N-3} + \cdots + b_1 2^0) \tag{3.25}$$

where $E$ = analog voltage
$N$ = number of binary digits
$b_i$ = state of $i$th binary digit

The encoded word usually is applied to a general-purpose computer in serial form but is applied to special-purpose high-speed computers in parallel form.

The Grey code is used in certain types of asynchronous converters where encoded data is read out of the converter continuously. This code allows all adjacent transitions to be accomplished by the change of a single digit only. Use of the Grey code greatly reduces the magnitude of transient errors in such cases.

Converters in radar systems normally have a complemented power-of-2 format for negative inputs. This simplifies both the converter and subsequent computations. In the complemented format, the converter counts up from the most negative value to zero and then continues to count up from zero to the most positive value. A sign bit indicates which half of the range applies. The process for the 2's complement may be described by

$$E = k(-b_N 2^{N-1} + b_{N-1}2^{N-2} + b_{N-2}2^{N-3} + \cdots + b_1 2^0) \tag{3.26}$$

and for the 1's complement by

$$E = k[-b_N(2^{N-1} - 1) + b_{N-1}2^{N-2} + b_{N-2}2^{N-3} + \cdots + b_1 2^0] \tag{3.27}$$

The 1's complement is seen to have two binary values for 0, but confusion may be eliminated by suppressing the one where all $b_i$'s are unity.

**Synchronization.** Converters operate in either a synchronous or an asynchronous mode. In the synchronous mode, the converter samples the analog data, decodes, and stores the result on command. An asynchronous converter, however, constantly tracks the changing analog input, and the digital output is in

effect sampled by the terminal equipment. The asynchronous converter should employ the Grey-code format to avoid the possibility of a large error should the output be sampled at the instant when digits are changing.

**Performance Characteristics**

*Signal Bandwidth.* The digital data used by the terminal equipment is always sampled. The bandwidth of this "digital signal" is limited to half the sampling frequency.

*Resolution.* The resolution of a converter is determined by the number of bits. For an $N$-bit converter, the resolution is $E_{max}/(2^N - 1)$ if the converter is truly monotonic, that is, if its response to an analog ramp is a uniform progression of binary numbers. This characteristic is usually realized with a slowly changing analog input but must be verified under pulsed conditions.

*Dynamic Range.* If the A/D converter is sampling the two components of the echo vector ($I$ and $Q$), each component contains half of the noise power and up to 100 percent of the signal power. The dynamic range is the maximum IF signal-to-noise ratio which can be handled by the A/D converter without saturating at any phase condition.

$$\text{Dynamic range (dB)} = 6N - 9 - 20 \log (\sigma/\text{LSB}) \tag{3.28}$$

where $N$ = number of bits including sign
$\sigma$ = rms noise in $I$ or $Q$
LSB = least-significant-bit voltage

*Quantization Noise.* The conversion of sampled noise voltages into integer numbers introduces an added random error which can be considered as an additional source of noise, requiring an increase in echo strength to achieve the desired detection probability if false-alarm probability is maintained constant.

$$\text{Quantization loss (dB)} = 10 \log \left[1 + \left(\frac{\text{LSB}}{\sigma}\right)^2\right] \qquad \sigma \geq \text{LSB} \tag{3.29}$$

*Sampling.* When the signal bandwidth is so great that the analog voltage changes significantly from sample to sample, the instantaneous signal may become distorted by the sampling process.[15] A slewing error results when the exponential charging is incomplete. An entirely separate lag error results from changes in signal amplitude during the sampling interval. Current flows in the storage capacitor, causing an $IR$ drop, which is still present when the switch is opened.

An additional error is introduced by the finite opening time of the switch. The signal tends to be averaged over this interval, and the sampled voltage does not correspond exactly to the voltage at the instant when the switch starts to open. The time required to open the switch is sometimes called the *aperture time*.

Design data specifying the slewing and lag errors is presented in Fig. 3.21. Practical circuits having $RC$ time constants of 3 ns and sampling intervals of 50 ns have been used in high-speed A/D conversion. The resultant slewing error is seen to be less than 0.001 percent, and, at a signal frequency of 0.5 MHz, the lag error is 0.46 percent. It should be emphasized that large sampling errors are not always fatal in a radar system. For example, in an MTI radar the error will repeat from one interpulse period to the next in stationary clutter, and it is therefore removed by subtraction in the canceler.

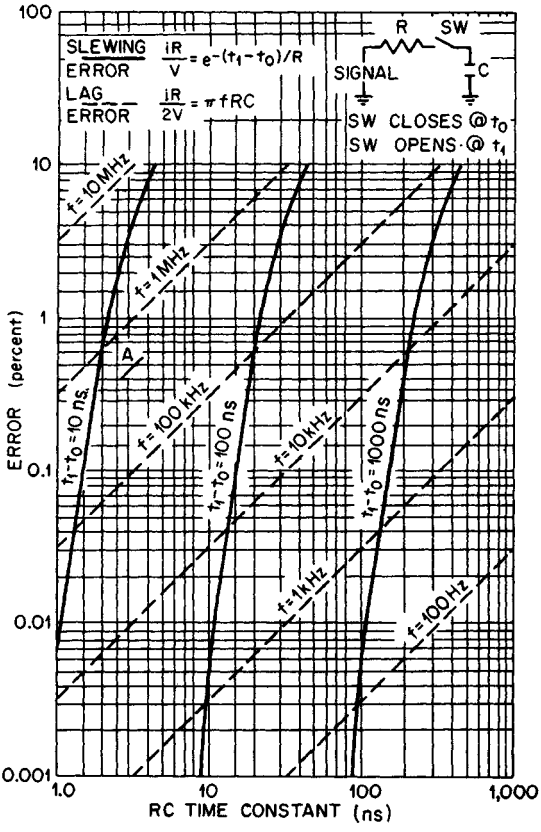


**FIG. 3.21** Sampling-circuit errors.

**Multiplexing.** *I* and *Q* data may be processed by the same A/D converter if its conversion rate limit is more than double the required sampling rate. It is essential that *I* and *Q* signals be sampled at the same instant of time; so such A/D converters generally employ a pair of sample-and-hold circuits, one to sample *I* and the other to sample *Q*. Their stored voltages are converted to digital numbers sequentially prior to the next sample time. Alternatively, a delay line can be employed for either *I* or *Q* to allow a single sample-and-hold to be employed, but pulse shape distortion in the delay line and timing error restrict this approach to applications which can tolerate such distortion (see Sec. 3.12).

## 3.12 I/Q DISTORTION EFFECTS AND COMPENSATION METHODS

**Gain or Phase Unbalance.** If the gains of the *I* and *Q* channels are not exactly equal or if their coho phase references are not exactly $\pi/2$ rad apart, an input signal at a single doppler frequency will create an output at the image

doppler frequency. If the ratio of voltage gains is $(1 \pm \Delta)$ or if the phase references differ by $(\pi/2 \pm \Delta)$, the ratio of the spurious image at $-f_d$ to the desired output of $f_d$ is $\Delta/2$ in voltage, $\Delta^2/4$ in power, or 20 (log $\Delta$) − 6 in decibels.

In simple MTI, which creates a symmetrical rejection notch to suppress clutter near zero doppler, the image frequency is not a problem; it is suppressed to the same degree as the true doppler. Early MTI radars exploited this tolerance of unbalance to simplify the hardware, processing only $I$ or $Q$, not both.

Modern radars often provide doppler filters to suppress moving clutter caused by movement of the radar platform or rain or sea clutter, and the image of the clutter in the rejection band can appear in the passband; so a high degree of balance must be preserved. Figure 3.22 shows the measured response of such a doppler filter with a large unbalance in $I/Q$ gain before and after compensation. Note that at those frequencies where the doppler sidelobes of the ideal filter and the image of the passband are of comparable magnitude, the response fluctuates widely, depending on the phase of the input signal.

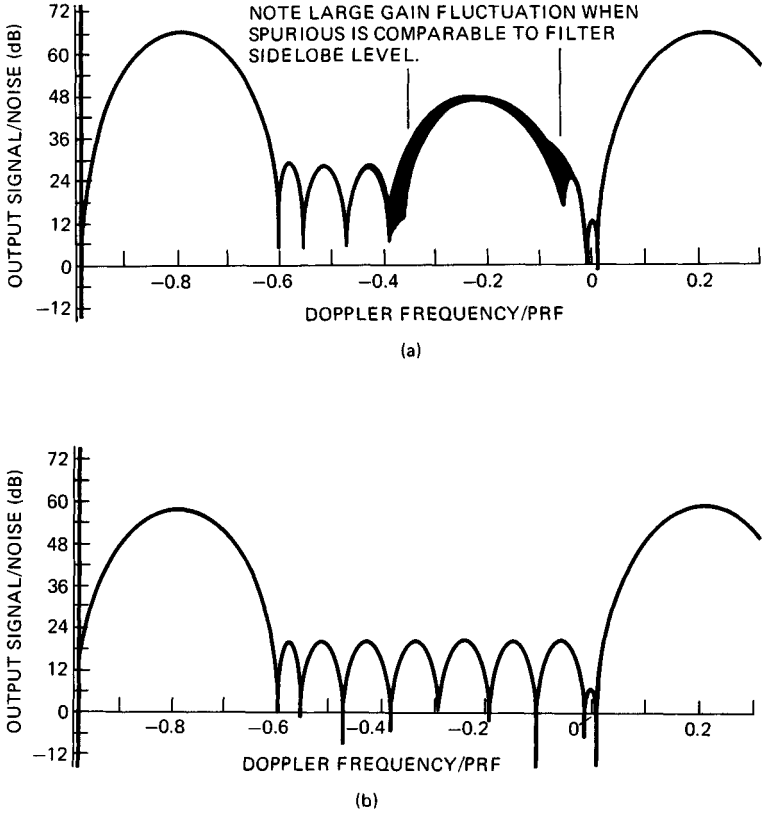


**FIG. 3.22** Measured doppler filter response with (*a*) 2 dB $I/Q$ gain unbalance generating image spurious ( $-f_D$) down 18 dB and (*b*) all spurious below noise.

The fluctuating response is the result of the vector addition of the two components: the image frequency and the sidelobe response of the filter to the input doppler. It represents a gain variation as a function of phase of the input signal. If echoes from a rainstorm have a velocity where this fluctuation is occurring, the amplitude statistics of the residue at the filter output will differ markedly from the input statistics, which are similar to noise. Amplitude-discrimination CFAR processes described in Sec. 3.13 are vulnerable to such a change in statistics; false-alarm rate in the rain area will increase significantly. To hold gain fluctuation to ±1 dB, the image must be suppressed 18 dB below the doppler filter sidelobes; so extremely low doppler sidelobes may not be a desirable characteristic. Phase-discrimination CFAR ignores all amplitude information and is more tolerant of spurious responses.

Error in gain and phase unbalance can be measured by injecting a doppler test tone into the receiver beyond the maximum range of interest, at a frequency corresponding to a null in the sidelobe response of an ideal filter (Fig. 3.22*b*) and near the peak response to the image (Fig. 3.22*a*).[16] The output of the filter represents the error, and a phase reference derived from a conjugate filter allows the error to be separated into gain and phase unbalance components. Two servos are used to drive this error down to the tolerable level of Fig. 3.22*b*.

Phase error may be corrected by a vernier phase shifter in one or both of the coho lines feeding the synchronous detector. Gain error may be corrected by a vernier change in gain in the IF, video, or digital stage of either or both $I$ and $Q$ channels. Video gain control often exaggerates the nonlinearity of those stages; digital control is preferable. It should be implemented by choosing a set of filter-weighting coefficients from a PROM appropriate for the measured gain unbalance.[16] It should not be implemented by scaling either $I$ or $Q$ data with a separate multiplier because this drastically increases the number of bits in the scaled input to the doppler filter. Truncation of the bits of lesser significance in this scaled data effectively causes the scaling factor to vary with signal level, resulting in a variety of unexpected and undesirable characteristics.

A measurement of the doppler spectrum at the center of an echo pulse, such as shown in Fig. 3.23*a*, indicates the degree of gain and phase unbalance compensation provided by the servos. However, as the following discussion will explain, the suppression of image doppler energy from moving clutter interference may be substantially less than indicated by this measurement at pulse center.

**Time Delay and Pulse Shape Unbalance.** If the responses of the $I$ and $Q$channels to the spectrum of the echo pulse are not identical, the two pulses will have slightly different pulse shapes or time delays. The gain and phase servos compensate for errors at the center of the receiver passband if they use a doppler test-tone pulse of substantially longer duration than the radar echo, but extreme care must be exercised in design of the video stages to ensure that this compensation is appropriate across the entire receiver passband. Optimum bandpass filtering should be at IF, where it affects $I$ and $Q$ channels identically, not at baseband. Video bandwidth should be many times wider than IF and controlled by precision components.

The test for this problem is a measurement of the desired output and the spurious image from a doppler-offset test pulse identical to the transmitted waveform. The measurement is performed at a multiplicity of sample points across the pulse until the image is no longer discernible on the leading and trailing edges. The image suppression of moving clutter echoes is

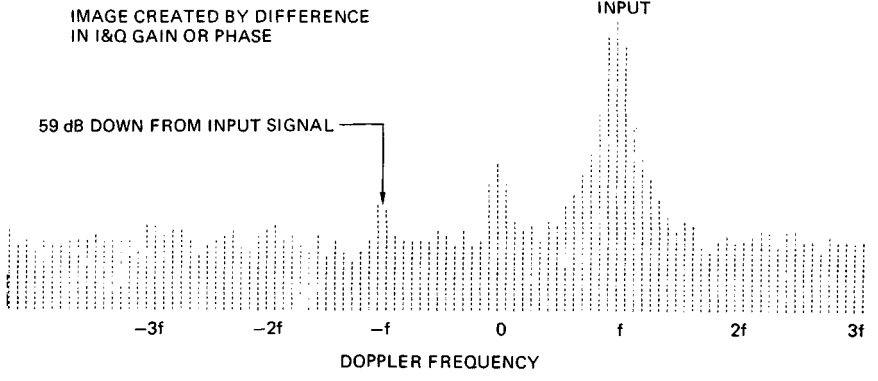


(a)

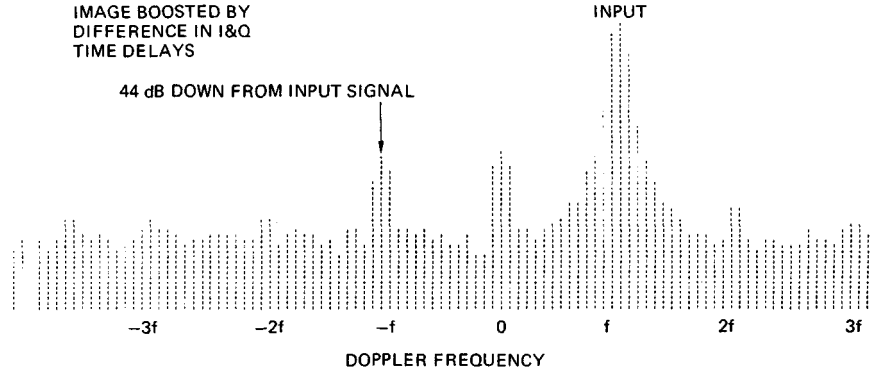


(b)

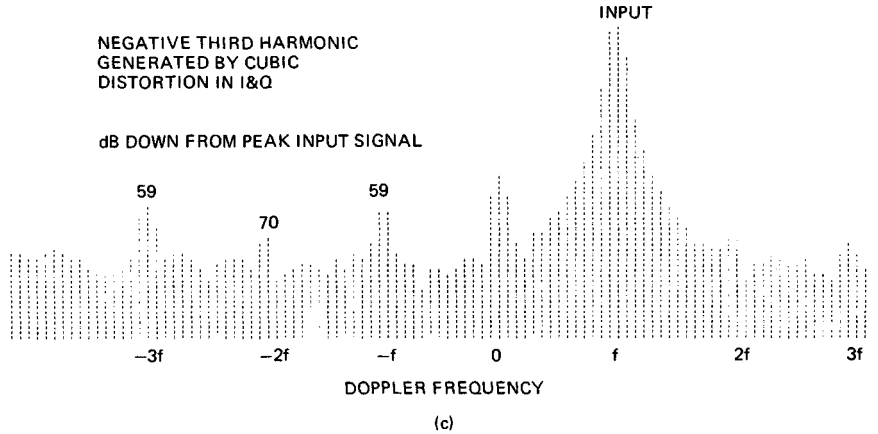


(c)

**FIG. 3.23** Spurious doppler frequencies generated in receiver. (*a*) Image created by difference in the $I$ and $Q$ gain or phase with sample at pulse center 49 dB above noise. (*b*) Image boosted by difference in $I$ and $Q$ time delays with sample at pulse edge 48 dB above noise. (*c*) Negative third harmonic generated by cubic distortion in $I$ and $Q$ with sample at pulse center 58 dB above noise.

$$10 \log \sum_{n=1}^{N} P_{Dn} - 10 \log \sum_{n=1}^{N} P_{In} \tag{3.30}$$

where $P_{Dn}$ = doppler power at sample point $n$
$P_{In}$ = image power at sample point $n$
$N$ = number of sample points

The problem is apparent in Fig. 3.23*b* with the sample point on the edge of the echo. The echo amplitude has been boosted so that the amplitude at the sample point is close to that in Fig. 3.23*a*, but the image response is 15 dB worse.

**Nonlinearity in *I* and *Q* Channels.** It is more difficult to achieve high dynamic range in the video stages (*I* and *Q*) than at IF or RF; so nonlinearity generally shows up first in these stages. Component tolerances often lead to somewhat different nonlinearities in *I* and *Q*, which can generate the variety of spurious doppler components shown in Fig. 3.23*c*, which involves a pulse within a few decibels of A/D saturation.

The ideal doppler input signal is

$$V = Ae^{j2\pi ft} = I + jQ \tag{3.31}$$

$$V = \frac{A}{2}(e^{j2\pi ft} + e^{-j2\pi ft}) - j\frac{A}{2}e^{j2\pi ft} - e^{j2\pi ft}) \tag{3.32}$$

Each video channel response can be expressed as a power series. For simplicity, only symmetrical distortion distortion will be considered. The A/D output, including a residual gain unbalance of $\Delta$, is

$$V' = I' + jQ' \tag{3.33}$$

$$I' = I - aI^3 - cI^5 \tag{3.34}$$

$$Q' = (1 + \Delta)Q - bQ^3 - dQ^5 \tag{3.35}$$

Substitution of Eqs. (3.34) and (3.35) into Eq. (3.32) yields the amplitudes of the doppler spectral components listed in Table 3.4. Note that if the nonlinearities in *I* and *Q* were identical ($a = b$; $c = d$), spurious components at $-5f$ and $+3f$ would not be present and image would be proportional to input signal amplitude. Spurious at zero doppler is not due to dc offset; it is the result of even-order nonlinearities which were omitted from the above equations. The negative third harmonic is the dominant spurious produced by nonlinearity.

**TABLE 3.4** Spurious Doppler Components Generated by *I*/*Q* Nonlinearity

| Doppler frequency | Amplitude of spectral component |
|---|---|
| $-5f$ | $A^5(c-d)/32$ |
| $-3f$ | $A^3(a+b)/8 + 5A^5(c+d)/32$ |
| $-f$ | $A(\Delta/2) + 3A^2(a-b)/8 + 5A^5(c-d)/16$ |
| (Input) $f$ | $A(1+\Delta/2) - 3A^2(a+b)/8 - 5A^5(c+d)/16$ |
| $+3f$ | $A^3(a-b)/8 + 5A^5(c-d)/32$ |
| $+5f$ | $A^5(c+d)/32$ |

**DC Offset.** Small signals and receiver noise can be distorted by an offset in the mean value of the A/D converter output unless the doppler filter suppresses this component. Actually, it is preferable to operate the A/D with an intentional offset because all bits switch between 0 and −1 and their accumulated errors make this voltage increment less predictable than others. An intentional offset can be subtracted at the A/D output, and it is the output of this subtractor which should be maintained close to zero.

False-alarm control in receivers without doppler filters is sometimes degraded by errors of a small fraction of the LSB; so correction is preferably applied at the analog input to the A/D rather than at the point where the error is sensed. An up-down counter reacting to polarity of noise (and ignoring zero) is an ideal error sensor; its most significant bits are converted to an analog voltage and added to the A/D input. A number of unused bits of lesser significance dictate the reaction time of the servo and prevent an interference pulse, no matter how strong, from having significant effect on the compensation.

## 3.13 CFAR DETECTION PROCESSES

**Application.** Many radars operate in an environment where the noise generated within its own receiver is not the dominant source of interference. Undesired echoes from rain and clutter and undesired signals from other radiating sources often exceed the receiver noise level. These sources of interference may completely obliterate the radar display, or they may overload either a computer that is attempting to track valid targets of interest or narrow-bandwidth data links to remote users.

The digital decision process usually involves threshold criteria both at the input and at the output of the digital processor. At each point, one can define the probability of detection of a desired target and the probability of false alarm from noise or one of the above sources of interference. An operator viewing a PPI display makes a somewhat similar decision, and so the concept of false alarms is applicable to most radar systems.

Either an operator or a digital processor would like to keep the false-alarm rate reasonably constant, having the radar automatically adjust its sensitivity as the intensity of interference varies. Receivers that have this property are called CFAR (constant false-alarm rate) receivers.

In older radars, the CFAR process was implemented in analog hardware, described in Sec. 5.8 of the 1970 edition of the handbook. In modern radars, digital implementation is virtually universal because it provides both greater accuracy and sophistication impractical by prior methods.

The CFAR processes described below are applied in the radar receiver's digital signal processor at every range sample point, independently of whether a target is present. This high processing rate makes special-purpose computers more economical than general-purpose programmable types. Implementation of two of the most widely employed CFAR processes will be described, and their effect on radar sensitivity, range resolution, and azimuth accuracy will be defined. Additional CFAR processes are discussed in Sec. 8.2.

If the target of interest is small in physical size compared with the range resolution cell of the radar and if the interference signals are distributed reasonably uniformly over a large area relative to the range resolution, one may exploit this fact to discriminate between them.

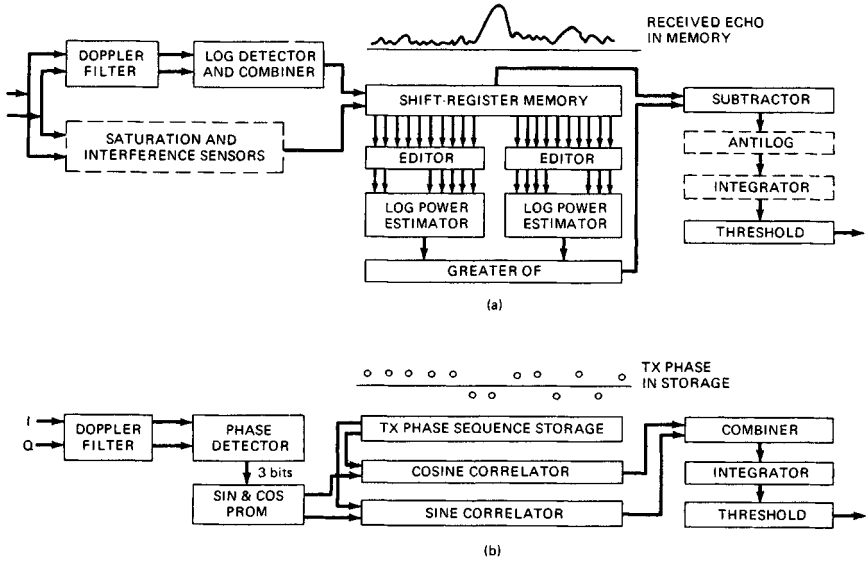


**FIG. 3.24** Modern digital signal processing for discriminating between point targets and distributed interference. (*a*) Amplitude-discrimination CFAR (cell-averaging). (*b*) Phase-discrimination CFAR (CPACS).

**Amplitude-Discrimination CFAR (Cell-Averaging CFAR).** The process shown in Fig. 3.24*a*, often called *range-averaging CFAR* or *cell-averaging CFAR*, is the digital descendant of the *log CFAR* described in the 1970 edition of the handbook (Sec. 5.8). It estimates the mean intensity of signals in neighboring range cells (the CFAR zone) and computes the signal-to-interference ratio of the central range sample. Because this estimate is based on a finite number of samples, it will fluctuate about the true value; the increased signal-to-noise ratio required to achieve a given detection probability, relative to that required if the estimated value did not fluctuate, is known as the *CFAR loss*.

Multiple interpulse periods of data may be integrated as the antenna beam scans past the target; so the estimate of interference can actually be based on a two-dimensional array of data. The CFAR loss decreases as the quantity of *independent* data samples increases, but adjacent data samples are rarely independent; the IF filter partially correlates adjacent noise samples in range, and a doppler filter (MTI) correlates noise samples from one interpulse period to the next. Equation (3.36), derived from Hansen's data,[17] shows the effect of these two filters on CFAR loss.

$$\text{Amplitude-discrimination CFAR loss (dB)} = \frac{5.5\chi}{(B_6 t_s)\left(\dfrac{M + h_M}{1 + h_M}\right)\left[\left(1 - \dfrac{D_6}{\text{PRF}}\right)\left(\dfrac{N + h_N}{1 + h_N}\right)\right]^i} \tag{3.36}$$

where $\chi = -\log P_{FA}$; $P_{FA} = 10^{-\chi}$
$M$ = number of range samples integrated
$N$ = number of interpulse periods integrated
$h$ = inefficiency factor of data integrated ($h = 0$ for power averaging, 0.09 for voltage averaging, and 0.65 for log averaging.)
$i$ = efficiency factor of postdetection integration ($i = 0$ for ratio following integration of $N$ pulses, and $i = 0.7$ for ratio preceding integration of $N$ pulses.)
$B_6$ = 6 dB bandwidth of IF filter, MHz
$t_s$ = sample spacing, μs, or $1/B_6$, whichever is smaller
$D_6$ = 6 dB width of rejection band of doppler filter, Hz
PRF = average pulse repetition frequency of data in doppler filter, Hz

Power averaging provides the minimum fluctuation in the estimate of interference. Averaging of voltage or logarithmic data produces greater fluctuation in the estimate, as indicated by the $h$ factors. The log data format is generally advantageous for four reasons:

**1.** Fewer bits cover the large dynamic range of radar echoes with adequate accuracy.

**2.** Signal-to-interference-ratio calculation requires only subtraction of log data rather than the more difficult division of voltage or power data.

**3.** Power summation of data in the CFAR zone is readily accomplished, using the log power combiner described in Sec. 3.8.

**4.** Integration of multiple interpulse periods may be accomplished in either power or voltage with equal facility.

Although integration prior to computing the ratio of signal to interference provides a lower CFAR loss ($i = 1$), the sequence shown in Fig. 3.24*a* is generally preferable because it can cope with variation in the level of interference from one interpulse period to the next. Intermittent interference (jamming or long pulses from other radars) produces no increase in false alarms and less sacrifice in sensitivity if integration follows the ratio calculation. If a 1-bit moving window is utilized as an integrator, the bracketed term in the denominator of Eq. (3.36) is omitted; the false-alarm rate at the *input* to the moving window defines $\chi$. When a doppler filter is involved, it must be remembered that the number of independent noise inputs is reduced; an $m$-out-of-$N$ detection criterion must be considered as an equivalent moving window with a criterion of

$$m\left(1 - \frac{D_6}{\text{PRF}}\right) \text{ out of } N\left(1 - \frac{D_6}{\text{PRF}}\right) \tag{3.37}$$

The size of the CFAR zone is limited by the size of the area where interference can be considered to have reasonably constant intensity. To maintain control of alarms in the center of severe rainstorms with typical diameters (3 dB) of 2 to 3 nmi, the CFAR zone should extend less than 1 nmi from the cell being examined. To prevent excessive alarms at the leading and trailing edges of the storm, it is advantageous to estimate interference separately in the "early" and "late" CFAR zones and use the "greater of" the two estimates rather than the average. The CFAR loss of the greater-of CFAR is only 0.1 to 0.3 dB more than one averaging the two estimates.[18]

The pulse spectrum of rain echoes is narrower than the noise spectrum; it is

the product of the IF bandwidth and the spectrum of the transmitted pulse. With reasonably optimum IF bandwidth, the reduction factor is $\sqrt{2}$. This causes more fluctuation in the estimate of rain echo level than in noise level, and the false-alarm rate in the rainstorm is higher due to this factor alone. If wind shear is inadequate to create an interference spectrum (rain plus noise) wider than noise alone at the output of a doppler filter, use of an integrator can cause another boost in the rain alarm rate due to this factor. Consequently, integrators should be used only in radars whose doppler filters create noise bandwidths narrower than the typical doppler spectrum of rain (15 to 30 kn).

If no postdetection integration is employed, the control of false alarms from sea clutter is very good with vertical or circular polarization but very poor with horizontal polarization, owing to a drastic difference in amplitude statistics of the echoes, which also depend upon compressed pulse width, beamwidth, etc. If the doppler filter is able to keep sea clutter residue equal to or lower than noise level, an integrator may be employed without creating false-alarm problems. The sea clutter residue spectrum is in part of the doppler band different from the output noise, and the composite spectrum is wider than noise alone. The false-alarm rate drops under conditions where sea clutter residue is comparable with noise because the composite interference has less correlation from one interpulse period to the next than noise alone.

The amplitude distribution of echoes from rain and the sea (with vertical or circular polarization and compressed pulse width exceeding 1 μs) does not differ significantly from noise, and the mean value varies slowly with range. Ground clutter varies much more rapidly with range; so the average clutter in neighboring cells is a poor estimate of the clutter in the center cell. Where the doppler filter is unable to suppress ground clutter well below noise, this CFAR process must be supplemented by other techniques to control alarms. These are discussed in Sec. 8.2 and in the "Clutter Map CFAR" subsection in this chapter.

**Phase-Discrimination CFAR (CPACS).** Another class of CFAR receivers completely obliterates all amplitude information in the echoes by employing limiters, with the normal noise level well above limit level.[19] These receivers discriminate between desired echoes and interference solely by the variation with time of the phase pattern at the limiter output, on the basis of how well it correlates with the phase code that was transmitted. This technique is often called the coded-pulse anticlutter system (CPACS) and comprises the elements so labeled in Fig. 3.1. Figure 3.24*b* explains the elements in greater detail.

In contrast to amplitude-discrimination techniques, phase-discrimination techniques have no problems with speed of response to changing intensity of interference. They sense only how well the echo matches a predetermined pattern of phase, and they can tolerate rapid and wide variation in signal strength: pulse interference from another radar, for example.

Fundamentally, limiting destroys some information and results in some degradation in performance. Detectability in noise is degraded by the limiting process,[20] but this loss drops to about 1 dB if the bandwidth-time product at the limiter exceeds 20. Similarly, limiting degrades the clutter attenuation capability of MTI radars that compare more than two pulses but have fewer than 20 hits per beamwidth. Consequently, doppler filtering must precede limiting to avoid this performance sacrifice in clutter. The digital phase detector described in Sec. 3.10 provides the required data for this CFAR process from a digital doppler filter; 3 bits of phase are adequate, while 2 bits add over 0.6 dB to CFAR loss. A PROM converts the phase ($\phi$) into $k \sin \phi$ and $k \cos \phi$ with $k = 7$ or 3.

Transmitter pulse length should not exceed the size of rainstorms (≈25 μs), and for these modest pulse lengths biphase or quadriphase codes are preferable to FM. The quadriphase code[5,6] is particularly advantageous, in that the impulse response of a gaussian IF filter is a close reproduction of the half-cosine subpulse of the code; the combination of the IF filter and digital correlator provides a nearly perfect matched filter. Range sampling loss and spectral splatter of the quadriphase code also are significantly superior to binary codes.

Both types of codes share the advantage of a simple CPACS decoder (a digital correlator requiring no multiplication). The CPACS decoder[13] merely adds $M_C$ adjacent data samples in range after rotating the phase of each sample 0°, ±90°, or 180°, corresponding to the transmitted phase code at that tap location but with opposite polarity. When the echo from a point target is centered in the digital correlator, these phase rotations cause data at all taps to have the same phase, creating the maximum output. Noise or distributed clutter produces random phase conditions, creating a mean power output lower by a factor of $M_C$, the number of subpulses in the code.

CFAR loss is described by Eq. (3.38), which is similar in form to that of amplitude-discrimination CFAR. The effect of an integrator on false-alarm control in rain or sea clutter is also similar.

Phase-discrimination CFAR loss (dB) =

$$1 + \frac{5.5\chi}{(M_C - 1)\left[\left(1 - \dfrac{D_6}{\text{PRF}}\right)\left(\dfrac{N + h_N}{1 + h_N}\right)\right]^i} \tag{3.38}$$

where all parameters are defined in the same manner as in amplitude-discrimination CFAR, except that $M_C$ = the number of subpulses in biphase or quadriphase code.

In contrast to amplitude-discrimination techniques, CPACS with a transmitter pulse length of 3.25 μs has been able to control alarms from clutter residue from the Swiss Alps without supplementary CFAR processes. The IF limiter is adjusted to begin limiting at a level where the clutter-to-noise ratio approaches the MTI improvement factor. The limiter splatters the scan modulation spectrum of the clutter so that the resulting residue has a broader doppler spectrum than the noise output of the MTI. CPACS ignores the extremely different amplitude statistics of the residue from limiting clutter, and the integrator reacts favorably to the broader residue spectrum.

**Effect on Range Resolution and Azimuth Accuracy.** The ability to detect two targets separated only in range can be seriously degraded by the CFAR processes described. Range resolution is generally dictated by the size of the CFAR zone, which is many times the width of the echo at the receiver output.

Probability of resolution ($Pr$) is the ratio of the probability of detecting both targets at specified separation to the probability of detecting both targets when widely separated. Resolution is the separation of equal Swerling Case 1 targets providing $Pr$ = 50 percent, if not otherwise specified.

Amplitude-discrimination CFAR is particularly vulnerable when the mean echo strengths of the two targets differ. The stronger target's echo located in the CFAR zone of the weaker, if included in the estimate of interference, will cause the weaker target to disappear. The effect is exaggerated by power averaging and absence of postdetection integration; under these conditions, Swerling 1 echoes of even equal

mean strength provide *zero* probability of detecting both targets on the same scan when the number of range samples integrated is less than or equal to 24.

The best solution to this problem is editing the strongest sample in the CFAR zone[21] and the neighboring samples before estimating the interference. Editing a single sample[21] is inadequate because the echo will generally affect a pair of samples; a strong echo will affect three or four samples.

Figure 3.25 shows the excellent probability of resolution provided by such editing. Without this editing, probability of resolution is *zero* with power averaging. Voltage averaging without editing provides poor probability of resolution; even the two echoes have equal mean strengths (dotted curve). Note that editing three samples provides greater immunity from degradation when one target has a considerably larger mean radar cross section than the other. Range samples are spaced 75 percent of the transmitted pulse width or 60 percent of the 6 dB width of the echo after IF filtering. Amplitude-discrimination CFAR with editing provides probability of resolution which depends primarily on the ratio of mean echo powers of the fluctuating targets; signal-to-noise ratio and range separation (within the CFAR zone) have little effect.

Phase-discrimination CFAR (CPACS) provides probability of resolution which depends primarily on range separation; signal-to-noise ratio and the ratio of mean echo powers have little effect. The larger echo provides the dominant phase information in the region where echoes overlap. The weaker echo provides only a portion of its code; in the extreme, its information content in the overlap region is completely obliterated. Even when targets have equal mean echo powers, their independent fluctuation characteristics generally signify that one echo is substantially stronger than the other; so probability of resolution is only moderately better than when target sizes are drastically different.

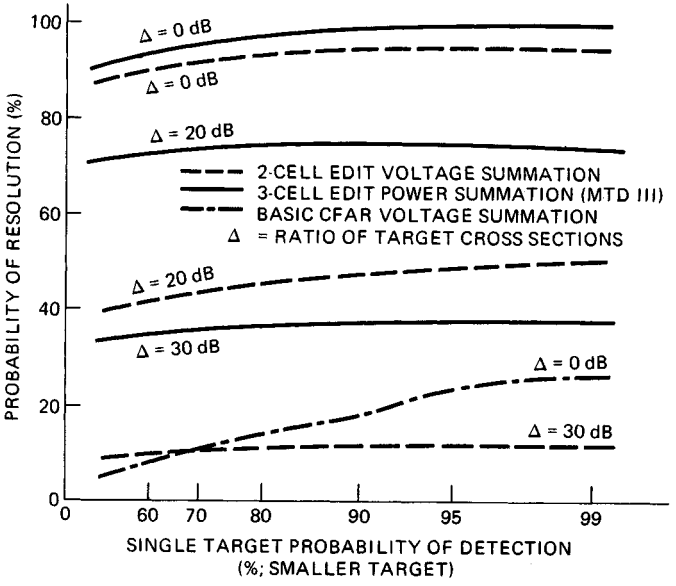


**FIG. 3.25** Three-cell editing improves the range resolution of two Swerling Case 1 targets within each other's CFAR zones (pair of 12-cell zones).

The effect of truncation of a portion of the weaker echo by a much stronger one is illustrated in Fig. 3.26 for three different overlap conditions *b*, *c*, and *d*. Quadriphase code 28B is employed in this example.[5,6] Loss of echo data in the overlap region causes a proportional reduction in the peak amplitude and some degradation in range sidelobes. When the peak falls below the detection threshold in Fig. 3.26*d*, the weaker echo is no longer detectable. Noise and the sidelobes of the stronger echo are not included in the presentation of Fig. 3.26; although their effects are small, one must select a code whose truncation sidelobes are well below the detection threshold to allow for their contribution. This is a factor in selecting good code which is often overlooked.

Range resolution of phase-discrimination CFAR can be estimated from Eq. (3.39).

$$\frac{\Delta t}{T} \approx \frac{4}{\sqrt{M_C}\left[\left(1 - \frac{D_6}{\text{PRF}}\right)\left(\frac{N + h_N}{1 + h_N}\right)\right]^i} \tag{3.39}$$

where $\Delta t$ = time separation of two echoes to achieve 50 percent probability of resolution
$T$ = transmitted-pulse duration

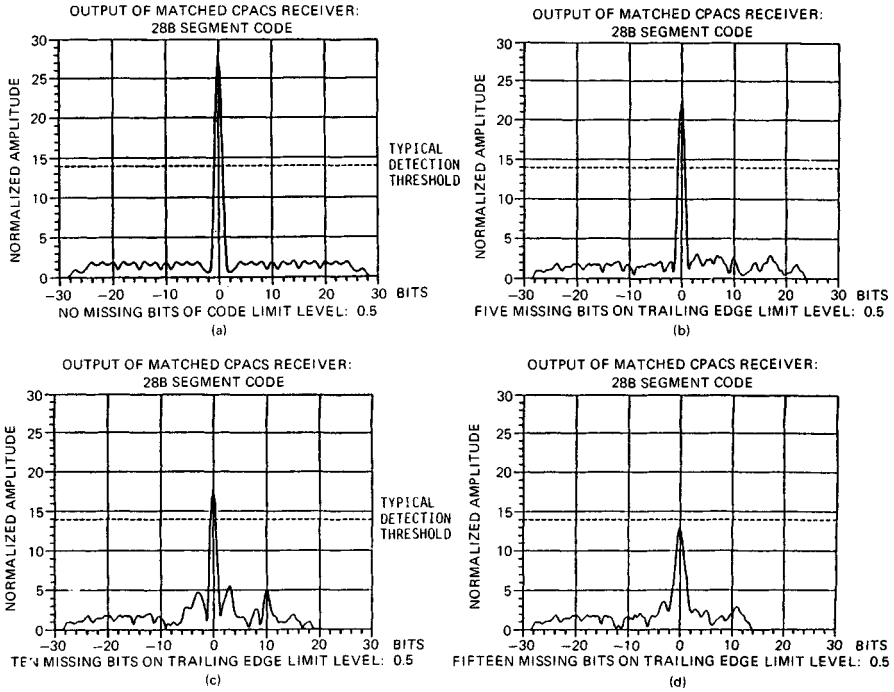


**FIG. 3.26** Effect of CPACS truncation of a weaker echo by a stronger target overlapping the trailing edge by a varying number of code segments: (*a*) 0; (*b*) 5; (*c*) 10; (*d*) 15.

Typically the answer is close to half of the transmitted-pulse duration.

Azimuth accuracy can be degraded if the azimuth of each target is calculated as the average of the first and last azimuths where the CFAR process detects the target. When two targets are separated in both range and azimuth, the effect of CFAR is to delay the initial detection of one target and advance the final detection of the other. The targets appear to be more widely separated in azimuth than they truly are. This problem can be avoided by using the CFAR process only for a detection decision, which initiates the transfer of a multiplicity of echo amplitudes to the data processor for determination of azimuth, range, and decision as to whether two targets are present with slightly different azimuths and/or ranges.

**Clutter Map CFAR.** A clutter map may be employed to provide better detectability of aircraft on near-tangential flight paths over clutter. The near-zero doppler echoes are suppressed by the doppler filter used to attenuate ground clutter, but terrain clutter does not cover large areas solidly. Screening of hills creates shadow areas where clutter is absent, and ability to detect aircraft in these areas, called *interclutter visibility*, is the primary reason for use of a clutter map CFAR.

Map cells must be spaced no farther apart than the azimuth beamwidth and compressed pulse width to provide maximum interclutter visibility. The mean echo voltage or power in each map cell over many scans is determined by exponential weighting, or integration; and the detection threshold is boosted above this value by a factor necessary to provide the desired probability of false alarm in noise. Clutter fluctuation from scan to scan is assumed to have statistics similar to noise *if no postdetection integration is employed*, as might be caused by windblown foliage.

Nitzberg[22] has calculated the CFAR loss of an exponentially weighted integrator with power input and feedback factor of $(1 - w)$. His results may be expressed as

$$\text{Clutter map CFAR loss (dB)} = \frac{5.5\chi}{1 + 2/w} \tag{3.40}$$

where $\chi$ is the exponent of the probability of false alarm. Map data is actually stored in logarithmic format to minimize the number of bits of data, but either voltage or power integration may be achieved by converting the equation to log format.

Clutter map CFAR is based on the assumption that clutter statistics are stationary. Moving rainstorms, jamming, pulses from other radars, and similar dynamically changing clutter conditions can cause an excessive alarm rate. Provisions to turn off this channel automatically in beams where excessive alarms occur are a necessity.

The clutter map may also be employed to sense locations where clutter echoes are too strong to be suppressed below noise by the doppler filter. To be effective, it must apply appropriate boost in the detection threshold at these locations and at neighboring azimuths as well;[23] the scanning radar beam creates residue on the leading and trailing edges of the beam, where echoes are weak but changing rapidly, as well as near the beam center.

## 3.14 DIPLEX OPERATION

**Benefits.** Diplex operation consists of two receivers which simultaneously process echoes from transmissions on two frequencies. Transmissions are usually nonoverlapping to avoid a 6 dB increase in peak power, but simultaneous reception of their echoes requires duplicate receivers. Although this doubles the cost of receivers and signal processors, the required average power of the transmitter or transmitters is reduced substantially; in most cases diplex operation reduces total cost.

Some transmitters, particularly solid-state, run closer to the peak power limit of the device than to the average power limit; their cost can be reduced if longer pulse durations can be tolerated. Diplex operation with unequal pulse lengths allows pulse duration to be more than doubled.

Minimum range dictates the shorter of the two pulse durations. Echoes cannot be received while transmission is occurring on either frequency; so the shorter pulse is the second transmission.

The effect of the highest-speed target on the compressed pulse restricts the longer-pulse duration. Digital phase codes and nonlinear FM provide low mismatch loss for targets of low doppler, but mismatch loss and range sidelobes of the compressed pulse degrade at maximum doppler; the longer the pulse, the more the degradation. Linear FM has a higher mismatch loss, but doppler has little effect on it or on range sidelobes. However, both linear and nonlinear FM produce a range offset as a function of doppler; they measure where the target was a fraction of a second ago or where it will be a fraction of a second in the future. These range displacements must match in the two receivers to within a small fraction of the compressed pulse width; otherwise, the sensitivity benefits of diplex operation are not totally achieved. Also, range accuracy may be degraded.

The sensitivity benefit of diplex operation for detecting Swerling 1 targets is shown in Fig. 3.27, increasing with $P_D$. For example, diplex operation achieves 90 percent $P_D$ with 2.6 dB less total signal power than simplex. The ability at least to double the duration of transmission provides a further benefit of a 3 dB or more reduction of peak power requirements. Assumptions made in deriving Fig. 3.27 are:

1. Echoes on the two frequencies are added in voltage or power prior to the detection decision rather than being subjected to individual detection decisions.

2. Separation of the two frequencies is sufficient to make their Swerling 1 fluctuations independent. This depends on the physical length of the target in the range dimension $\ell_r$. The minimum frequency separation is 150 MHz/$\ell_r$ (m); 25 MHz will maintain the diplex benefit for aircraft longer than 6 m (20 ft).

3. Equal energy is transmitted in both pulses. A 2:1 unbalance sacrifices only 0.2 dB of the benefit at 90 percent $P_D$.

**Recommended Implementation.** The echoes can be amplified in a wideband low-noise RF amplifier but should be separated into two individual channels prior to the mixer, using RF filters. Where rapid tuning or frequency agility is required, a switched filter bank is the preferred method. YIG filters are sometimes employed in radars which do not aim for high clutter attenuation. If both echoes were processed by the same mixer, with separation occurring at IF, the spurious signals generated in this nonlinear device could seriously degrade clutter attenuation. The number of spurious frequencies is much larger than those shown in Fig. 3.2, and they can be intolerably strong.

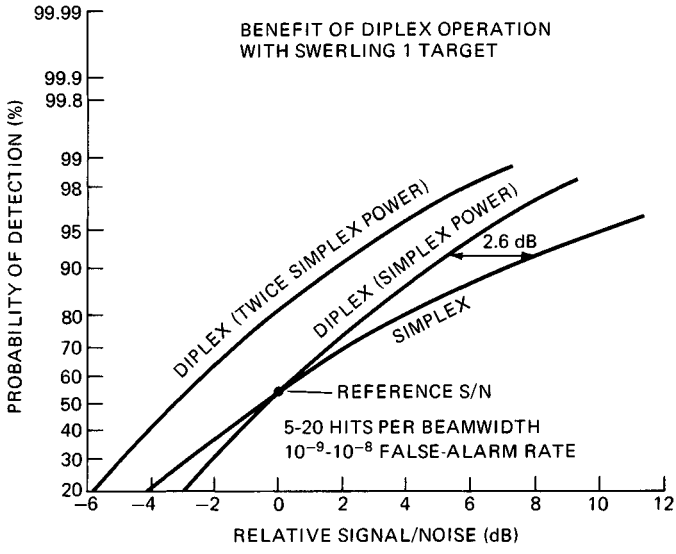


**FIG. 3.27** Diplex operation improves the sensitivity of the receiver.

Although separation prior to mixing solves the largest spurious problem, it does not eliminate similar nonlinearity effects in the shared RF amplifier. To avoid problems here, the separation of the two frequencies must be an integer multiple of the clock frequency used for timing the transmissions. This ensures that overlapping clutter echoes from stationary objects have the same relative phase after each transmission; so the effect of distortions in the RF amplifier is repeated.

Two operating frequencies can be provided by a single stalo, using both upper and lower sidebands.[24] By making the IF frequencies of the two receivers differ by a few megahertz, each stalo frequency can provide four operating frequency choices. This reduces the number of stalo choices which must be provided to meet specified tuning requirements. If each IF channel is designed to operate on a different sideband, the transmitted frequencies are separated by the *sum* of the two IFs. Use of a single sideband would separate the transmitted frequencies by the *difference* in the two IFs; this may not provide the full benefit of diplex operation with small aircraft, since condition 2 above might not be satisfied.

## REFERENCES

1. Brown, T. T.: Mixer Harmonic Chart, *Electron. Buyer's Guide*, pp. R46, R47, June 1954.
2. Barber, M. R.: A Numerical Analysis of the Tunnel Diode Frequency Converter, *IEEE Trans.*, vol. MTT-13, pp. 663–670, September 1965.
3. Gambling, W. R., and S. B. Mallick: Tunnel-Diode Mixers, *Proc. IEEE*, pp. 1311–1318, July 1965.

4. Rice, S. O.: Response of a Linear Rectifier to Signal and Noise, *J. Acoust. Soc. Am.*, vol. 16, p. 164, 1944.
5. Taylor, J. W., Jr., and H. J. Blinchikoff: The Quadriphase Code—A Radar Pulse Compression Signal with Unique Characteristics, *IEE Conf. Publ.* 281, pp. 315–319, London, October 1987.
6. Taylor, J. W., Jr., and H. D. Blinchikoff: Quadriphase Code—A Radar Pulse Compression Signal with Unique Characteristics, *IEEE Trans.*, vol. AES-24, pp. 156–170, March 1988.
7. Solms, S. J.: Logarithmic Amplifier Design, *IRE Trans.*, vol. I-8, pp. 91–96, 1959.
8. Croney, J.: A Simple Logarithmic Receiver, *Proc. IRE*, vol. 39, pp. 807–813, July 1951.
9. Rubin, S. N.: A Wide-Band UHF Logarithmic Amplifier, *IEEE J. Solid State Circuits*, vol. 1, pp. 74–81, December 1966.
10. Gardner, F. M.: "Phaselock Techniques," John Wiley & Sons, New York, 1967.
11. Calaway, W.: The Design of Wideband Limiting Circuits, *Electron. Design News*, vol. 10, pp. 42–53, December 1965.
12. Highleyman, W. H., and E. S. Jacob: An Analog Multiplier Using Two Field Effect Transistors, *IRE Trans.*, vol. CS-10, pp. 311–317, September 1962.
13. Taylor, J. W., Jr.: Constant False Alarm Rate Radar System and Method of Operating the Same, U.S. Patent 4,231,005, October 1980.
14. Daley, F. D.: Analog-to-Digital Conversion Techniques, *Electro-Technol. (New York)*, vol. 79, pp. 34–39, May 1987.
15. Barr, P.: Voltage to Digital Converters and Digital Voltmeters, *Electromech. Design*, vol. 9, pp. 301–310, January 1965.
16. Taylor, J. W., Jr.: System and Method of Compensating a Doppler Processor for Input Unbalance and an Unbalance Sensor for Use Therein, U.S. Patent 4,661,229, October 1986.
17. Hansen, V. G.: Constant False Alarm Rate Processing in Search Radars, "Radar—Present and Future," *IEE Conf. Publ.* 105, London, October 1973.
18. Hansen, V. G., and J. H. Sawyers: Detectability Loss Due to "Greatest of" Selection in a Cell-Averaging CFAR, *IEEE Trans.*, vol. AES-16, pp. 115–118, January 1980.
19. Bogotch, S. E., and C. E. Cook: The Effect of Limiting on the Detectability of Partially Time-Coincident Pulse Compression Signals, *IEEE Trans.*, vol. MIL-9, pp. 17–24, January 1965.
20. Bello, P., and W. Higgins: Effect of Hard Limiting on the Probabilities of Incorrect Dismissal and False Alarm at the Output of an Envelope Detector, *IRE Trans.*, vol. IT-7, pp. 60–66, April 1961.
21. Richard, J. T., and G. M. Dillard: Adaptive Detection Algorithms for Multiple-Target Situations, *IEEE Trans.*, vol. AES-13, pp. 338–343, July 1977.
22. Nitzberg, R.: Clutter Map CFAR Analysis, *IEEE Trans.*, vol. AES-22, pp. 419–421, July 1986.
23. Taylor, J. W., Jr.: Point Clutter Threshold Determination for Radar Systems, U.S. Patent 4,713,664, December 1987.
24. Taylor, J. W., Jr.: Double Sideband Pulse Radar, U.S. Patent 4,121,212, October 1978.